Supporting Material

Mechanisms by which cytoplasmic calcium wave propagation and alternans are generated in cardiac atrial myocytes lacking t-tubules – insights from a simulation study

Qince Li, Stephen C. O'Neill, Tao Tao, Yatong Li, David Eisner, and Henggui Zhang

GLOSSARY

$[Ca^{2+}]_i$	Myoplasmic Ca^{2+} concentration
$[Ca^{2+}]_{J/NJ}$	Ca^{2+} concentration in junctional and non-junctional compartments adjacent to RyRs
$[Ca^{2+}]_o$	Extracellular Ca^{2+} concentration
$[Ca^{2+}]_{rel}$	Ca^{2+} concentration in junctional SR
$[Ca^{2+}]_{up}$	Ca^{2+} concentration in network SR
$[CQ]_{tot}$	Total calsequestrin concentration
$[CM]_{tot}$	Total calmodulin concentration
d_L	Activation gating variable for $I_{Ca,L}$
$d_{L,\infty}$	Steady-state d_L
d_{NaCa}	Denominator constant for I_{NaCa}
d_T	Activation gating variable for $I_{Ca,T}$
$d_{T,\infty}$	Steady-state d_T
$E_{Ca,L}$	Reversal potential of $I_{Ca,L}$
$E_{Ca,T}$	Reversal potential of $I_{Ca,T}$
f_{CMi}	Fractional occupancy of calmodulin by $[Ca^{2+}]_i$
$f_{CMJ/NJ}$	Fractional occupancy of calmodulin by $[Ca^{2+}]_{J/NJ}$
f_{CQ}	Fractional occupancy of calsequestrin by $[Ca^{2+}]_{rel}$
f_L	Inactivation gating variable for $I_{Ca,L}$
$f_{L,\infty}$	Steady-state f_L
f_T	Inactivation gating variable for $I_{Ca,T}$
$f_{T,\infty}$	Steady-state f_T
f_{TC}	Fractional occupancy of the troponin Ca^{2+} site by $[Ca^{2+}]_i$

f_{TMC}	Fractional occupancy of the troponin Mg^{2+} site by $[Ca^{2+}]_i$
f_{TMM}	Fractional occupancy of the troponin Mg^{2+} site by Mg^{2+}
F	Faraday constant
$g_{Ca,L}$	Maximum $I_{Ca,L}$ conductance
$g_{Ca,T}$	Maximum $I_{Ca,T}$ conductance
$I_{Ca,L}$	L-type Ca^{2+} current
$I_{Ca,P}$	Sarcolemmal Ca^{2+} pump
$I_{Ca,T}$	T-type Ca^{2+} current
I_{NaCa}	Na^{+}-Ca^{2+} exchange current (NCX)
J_{Ca_diff}	Ca^{2+} diffusion flux from junctional/non-junctional space to myoplasm
J_{Ca_J/NJ_diff}	Ca^{2+} diffusion flux between junctional/non-junctional spaces
$J_{Ca\_up\_diff}$	Ca^{2+} diffusion flux between neighbouring network SR
J_{rel}	Ca^{2+} release flux from the junctional SR to junctional/non-junctional space
J_{tr}	Ca^{2+} transfer flux from the network SR to junctional SR
J_{up}	Ca^{2+} uptake flux from the myoplasm to network SR
k_{bCM}	Ca^{2+} dissociation constant for calmodulin
k_{bCQ}	Ca^{2+} dissociation constant for calsequestrin
k_{bTC}	Ca^{2+} dissociation constant for troponin-Ca complex
k_{bTMC}	Ca^{2+} dissociation constant for troponin-Mg complex
k_{bTMM}	Mg^{2+} dissociation constant for troponin-Mg complex
k_{fCM}	Ca^{2+} association constant for calmodulin
k_{fCQ}	Ca^{2+} association constant for calsequestrin
k_{fTC}	Ca^{2+} association constant for troponin
k_{fTMC}	Ca^{2+} association constant for troponin-Mg complex

k_{fTMM}	Mg^{2+} association constant for troponin-Mg complex
k_{NaCa}	Scaling factor for I_{NaCa}
K_{rel}	Half-maximal $[Ca^{2+}]_{J/NJ}$ for Ca^{2+} release from the junctional SR
K_{up}	Half-maximal $[Ca^{2+}]_i$ for Ca^{2+} uptake by Ca^{2+}-pump in the network SR
$[Na^+]_i$	Intracellular Na^+ concentration
$[Na^+]_0$	Extracellular Na^+ concentration
P_{rel}	Rate constant for Ca^{2+} release from the junctional SR
P_{up}	Rate constant for Ca^{2+} uptake by Ca^{2+}-pump in the network SR
R	Universal gas constant
RyR	Ryanodine receptor
SR	Sarcoplasmic reticulum
t	Time
T	Absolute temperature
$[TC]_{tot}$	Total concentration of troponin-Ca complex
$[TMC]_{tot}$	Total concentration of troponin-Mg complex
V	Membrane potential
V_{cell}	Cell volume
V_i	Myoplasmic volume
$V_{J/NJ}$	Volume of junctional and non-junctional compartments
V_{rel}	Volume of junctional SR
V_{up}	Volume of network SR
y_{NaCa}	Position of energy barrier controlling voltage dependence of I_{NaCa}
α_{dL}	Opening rate constant of d_L
α_{dT}	Opening rate constant of d_T

α_{fL} Opening rate constant of f_L

α_{fT} Opening rate constant of f_T

β_{dL} Closing rate constant of d_L

β_{dT} Closing rate constant of d_T

β_{fL} Closing rate constant of f_L

β_{fT} Closing rate constant of f_T

τ_{Ca_J/NJ_diff} Time constant for Ca^{2+} diffusion between neighboring junctional/non-junctional space

$\tau_{Ca\_up\_diff}$ Time constant for Ca^{2+} diffusion between neighboring network SR units

τ_{diff_Ca} Time constant for Ca^{2+} diffusion from junctional/non-junctional space to myoplasm

τ_{dL} Time constant of d_L

τ_{dT} Time constant of d_T

τ_{fL} Time constant of f_L

τ_{fT} Time constant of f_T

τ_{tr} Time constant for Ca^{2+} transfer from the network SR to junctional SR

MODEL EQUATIONS

L-type Ca^{2+} channel current

$$I_{Ca,L} = g_{Ca,L} \times (f_L d_L + \frac{0.006}{1.0 + e^{\frac{-(V+14.1)}{6.0}}}) \times (V - E_{Ca,L})$$

$$\alpha_{d_L} = -14.19 \times \frac{V + 35.0}{e^{\frac{-(V+35.0)}{2.5}} - 1} - \frac{42.45V}{e^{-0.208V} - 1.0}$$

$$\beta_{d_L} = 5.71 \times \frac{V - 5}{e^{0.4(V-5)} - 1.0}$$

$$\tau_{d_L} = \frac{1.0}{\alpha_{\mathrm{dL}} + \beta_{dL}}$$

$$d_{L\infty} = \frac{1.0}{1.0 + e^{\frac{-(V+23.1)}{6.0}}}$$

$$\frac{dd_L}{dt} = \frac{d_{L\infty} - d_L}{\tau_{d_L}}$$

$$\alpha_{f_L} = 3.12 \times \frac{V + 28.0}{e^{\frac{V+28.0}{4.0}} - 1.0}$$

$$\beta_{f_L} = \frac{25.0}{1.0 + e^{\frac{-(V+28.0)}{4.0}}}$$

$$\tau_{f_L} = \frac{1.0}{\alpha_{fL} + \beta_{fL}}$$

$$f_{L\infty} = \frac{1.0}{1.0 + e^{\frac{V+45.0}{5.0}}}$$

$$\frac{df_L}{dt} = \frac{f_{L\infty} - f_L}{\tau_{f_L}}$$

T-type Ca^{2+} channel current

$$I_{Ca,T} = g_{Ca,T} \times f_T \times d_T \times (V - E_{Ca,T})$$

$$\alpha_{d_T} = 1068e^{\frac{V+26.3}{30}}$$

$$\beta_{d_T} = 1068e^{-\frac{V+26.3}{30}}$$

$$\tau_{d_T} = \frac{1.0}{\alpha_{\mathrm{dT}} + \beta_{dT}}$$

$$d_{T\infty} = \frac{1.0}{1.0 + e^{\frac{-(V+37)}{6.8}}}$$

$$\frac{dd_T}{dt} = \frac{d_{T\infty} - d_T}{\tau_{d_T}}$$

$$\alpha_{f_T} = 15.3 \times e^{-\frac{V+71.7}{83.3}}$$

$$\beta_{f_T} = 15e^{\frac{V+71.7}{15.38}}$$

$$\tau_{f_T} = \frac{1.0}{\alpha_{fT} + \beta_{fT}}$$

$$f_{T\infty} = \frac{1.0}{1.0 + e^{\frac{V+71}{9}}}$$

$$\frac{df_T}{dt} = \frac{f_{T\infty} - f_T}{\tau_{f_T}}$$

Na^{+}-Ca^{2+} exchange current

$$I_{NaCa} = K_{NaCa} \bullet \frac{[Na^+]_i^3 \bullet [Ca^{2+}]_o \bullet e^{0.03743 V y_{NaCa}} - [Na^+]_o^3 \bullet [Ca^{2+}]_{J/NJ} \bullet e^{0.03743 V (y_{NaCa} - 1.0)}}{1.0 + d_{NaCa} \bullet ([Na^+]_i^3 \bullet [Ca^{2+}]_o + [Na^+]_o^3 \bullet [Ca^{2+}]_{J/NJ})}$$

Intracellular Ca^{2+} Dynamics

Ca^{2+} diffusion flux

$$J_{Ca\_diff} = \frac{[Ca^{2+}]_{J/NJ} - [Ca^{2+}]_i}{\tau_{diff\_Ca}}$$

Ca^{2+} diffusion flux between neighboured elements *For each of the coupled element array, indexed by k (k varies between 1 to 13):*

$$J_{Ca\_J/NJ\_diff} = \frac{[Ca^{2+}]_{J/NJ}^{(k-1)} + [Ca^{2+}]_{J/NJ}^{(k+1)} - 2.0[Ca^{2+}]_{J/NJ}^{(k)}}{\tau_{Ca\_J/NJ\_diff}}$$

$$J_{Ca\_up\_diff} = \frac{[Ca^{2+}]_{up}^{(k-1)} + [Ca^{2+}]_{up}^{(k+1)} - 2.0[Ca^{2+}]_{up}^{(k)}}{\tau_{Ca\_up\_diff}}$$

SR Ca^{2+} regulation

$$J_{rel} = P_{rel} \bullet ([Ca^{2+}]_{rel} - [Ca^{2+}]_{J/NJ}) \bullet \frac{[Ca^{2+}]_{J/NJ}^{\ 2}}{[Ca^{2+}]_{J/NJ}^{\ 2} + K_{rel}^{\ 2}}$$

$$J_{up} = P_{up} \bullet \frac{[Ca^{2+}]_i}{[Ca^{2+}]_i + K_{up}}$$

$$J_{tr} = \frac{[Ca^{2+}]_{up} - [Ca^{2+}]_{rel}}{\tau_{tr}}$$

Ca^{2+} concentrations

$$\frac{d[Ca^{2+}]_i}{dt} = \frac{J_{Ca\_diff} \bullet V_{J/NJ} - J_{up} \bullet V_{up} - I_{CaP}/(2.0 \times F)}{V_i} - 1.0 \times ([CM]_{tot} \bullet f_{CMi\_rate} + [TC]_{tot} \bullet f_{TC\_rate} + [TMC]_{tot} \bullet f_{TMC\_rate})$$

$$\frac{d[Ca^{2+}]_{J/NJ}^{(periphery)}}{dt} = \frac{-(I_{CaL} + I_{CaT} - 2.0I_{NaCa})/(2.0\times F) + J_{rel} \bullet V_{rel}}{V_{sub}} - J_{Ca\_diff} + J_{Ca\_J/NJ\_diff} - [CM]_{tot} \bullet f_{CMs\_rate}$$

$$\frac{d[Ca^{2+}]_{J/NJ}^{(centre)}}{dt} = \frac{J_{rel} \bullet V_{rel}}{V_{sub}} - J_{Ca\_diff} + J_{Ca\_J/NJ\_diff} - [CM]_{tot} \bullet f_{CMs\_rate}$$

$$\frac{d[Ca^{2+}]_{rel}}{dt} = J_{tr} - J_{rel} - [CQ]_{tot} \bullet f_{CQ\_rate}$$

$$\frac{d[Ca^{2+}]_{up}}{dt} = J_{up} - J_{tr} \bullet \frac{V_{rel}}{V_{up}}$$

Ca^{2+} buffering

$$\frac{df_{TC}}{dt} = Kf_{TC} \bullet [Ca^{2+}]_i \bullet (1 - f_{TC}) - Kb_{TC} \bullet f_{TC}$$

$$\frac{df_{TMC}}{dt} = Kf_{TMC} \bullet [Ca^{2+}]_i \bullet (1 - f_{TMC} - f_{TMM}) - Kb_{TMC} \bullet f_{TMC}$$

$$\frac{df_{TMM}}{dt} = Kf_{TMM} \bullet [Mg^{2+}]_i \bullet (1 - f_{TMC} - f_{TMM}) - Kb_{TMM} \bullet f_{TMM}$$

$$\frac{df_{CMi}}{dt} = Kf_{CM} \bullet [Ca^{2+}]_i \bullet (1 - f_{CMi}) - Kb_{CM} \bullet f_{CMi}$$

$$\frac{df_{CMJ/NJ}}{dt} = Kf_{CM} \bullet [Ca^{2+}]_{J/NJ} \bullet (1 - f_{CMJ/NJ}) - Kb_{CM} \bullet f_{CMJ/NJ}$$

$$\frac{df_{CQ}}{dt} = Kf_{CQ} \bullet [Ca^{2+}]_{rel} \bullet (1 - f_{CQ}) - Kb_{CQ} \bullet f_{CQ}$$

MODEL PARAMETER VALUES

Model Parameters	Values
$[Ca^{2+}]_o$ (mM)	2
$[CM]_{tot}$ (mM)	0.045
$[CQ]_{tot}$ (mM)	10
d_{NaCa}	0.0001
$E_{Ca,L}$ (mV)	46.4
$E_{Ca,T}$ (mV)	45
F ($C \cdot M^{-1}$)	96,484.60
$g_{Ca,L}$	0.052709184
$g_{Ca,T}$	0.0138823
k_{bCM} (ms^{-1})	0.542
k_{bCQ} (ms^{-1})	0.445
k_{bTC} (ms^{-1})	0.446
k_{bTMC} (ms^{-1})	0.00751
k_{bTMM} (ms^{-1})	0.751
k_{fCM} ($mM^{-1} \cdot ms^{-1}$)	227.7
k_{fCQ} ($mM^{-1} \cdot ms^{-1}$)	0.534
k_{fTC} ($mM^{-1} \cdot ms^{-1}$)	88.8
k_{fTMC} ($mM^{-1} \cdot ms^{-1}$)	227.7
k_{fTMM} ($mM^{-1} \cdot ms^{-1}$)	2.277
k_{NaCa}	2.20896E-5
K_{rel} (mM)	0.0012
K_{up} (mM)	0.00045
$[Na^+]_i$ (mM)	8
$[Na^+]_o$ (mM)	140
P_{rel} (ms^{-1})	1.8
P_{up} (mM/ms)	0.005
R ($J \cdot mol^{-1} \cdot K^{-1}$)	8.314472
T (K)	310
$[TC]_{tot}$ (mM)	0.031
$[TMC]_{tot}$ (mM)	0.062

V_i (pl)	13
$V_{J/NJ}$ (pl)	0.84
V_{rel} (pl)	0.2352
V_{up} (pl)	1.624
y_{NaCa}	0.5
τ_{tr} (ms)	60
τ_{diff_Ca} (ms)	0.04
τ_{Ca_J/NJ_diff} (ms)	0.4
$\tau_{Ca\_up\_diff}$ (ms)	600

INITIAL CONDITIONS

Model Variables	Initial Values
V, mV	-40
f_L	0.268941
d_L	0.05643
f_T	0.030935
d_T	0.391461
$[Ca^{2+}]_i$, mM	0.000038
$[Ca^{2+}]_{J/NJ}$, mM	0.000056
$[Ca^{2+}]_{rel}$, mM	1.613677
$[Ca^{2+}]_{up}$, mM	1.613684
f_{CMi}	0.015683
$f_{CMJ/NJ}$	0.02313
f_{CQ}	0.607183
f_{TC}	0.007498
f_{TMC}	0.138813
f_{TMM}	0.760791

MODEL VALIDATION

1. Effect of increasing Ca^{2+} influx by elevating $[Ca^{2+}]_o$

It has been shown that an increase in Ca^{2+} influx by elevating $[Ca^{2+}]_o$ helps to sustain full Ca^{2+} wave propagation towards the central region and reduces the $[Ca^{2+}]_i$ spatial heterogeneity in atrial cells (1). This experimental observation was reproduced by the model for validation purposes. In the model, an augmented Ca^{2+} influx was simulated by elevating the extracellular Ca^{2+} concentration ($[Ca^{2+}]_o$) from 1 mM to 10 mM (Fig. S1). Such an increase in Ca^{2+} influx produced a larger $[Ca^{2+}]_i$ transient in the peripheral region, and thus produced an enhanced Ca^{2+} wave. Fig. S1A presents a line scan image of the $[Ca^{2+}]_i$ transient across the cell. In this figure, the cell was paced under control conditions for several beats before $[Ca^{2+}]_o$ was increased. The Ca^{2+} wave propagation was promoted after increasing $[Ca^{2+}]_o$ (Fig. S1A). Fig. S1B and C represented the time courses of the $[Ca^{2+}]_i$ transient and SR Ca^{2+} content ($[Ca^{2+}]_{SR}$) recorded from sites near the periphery (black) and in the central regions (red) for control (Fig. S1B) and increased $[Ca^{2+}]_o$ (Fig. S1C) conditions. It was shown that enhanced inward Ca^{2+} wave propagation was evoked by increasing $[Ca^{2+}]_o$ (Fig. S1C). These simulation results match the experimental data of Mackenzie *et al.* (1) as shown in Inset A and B .

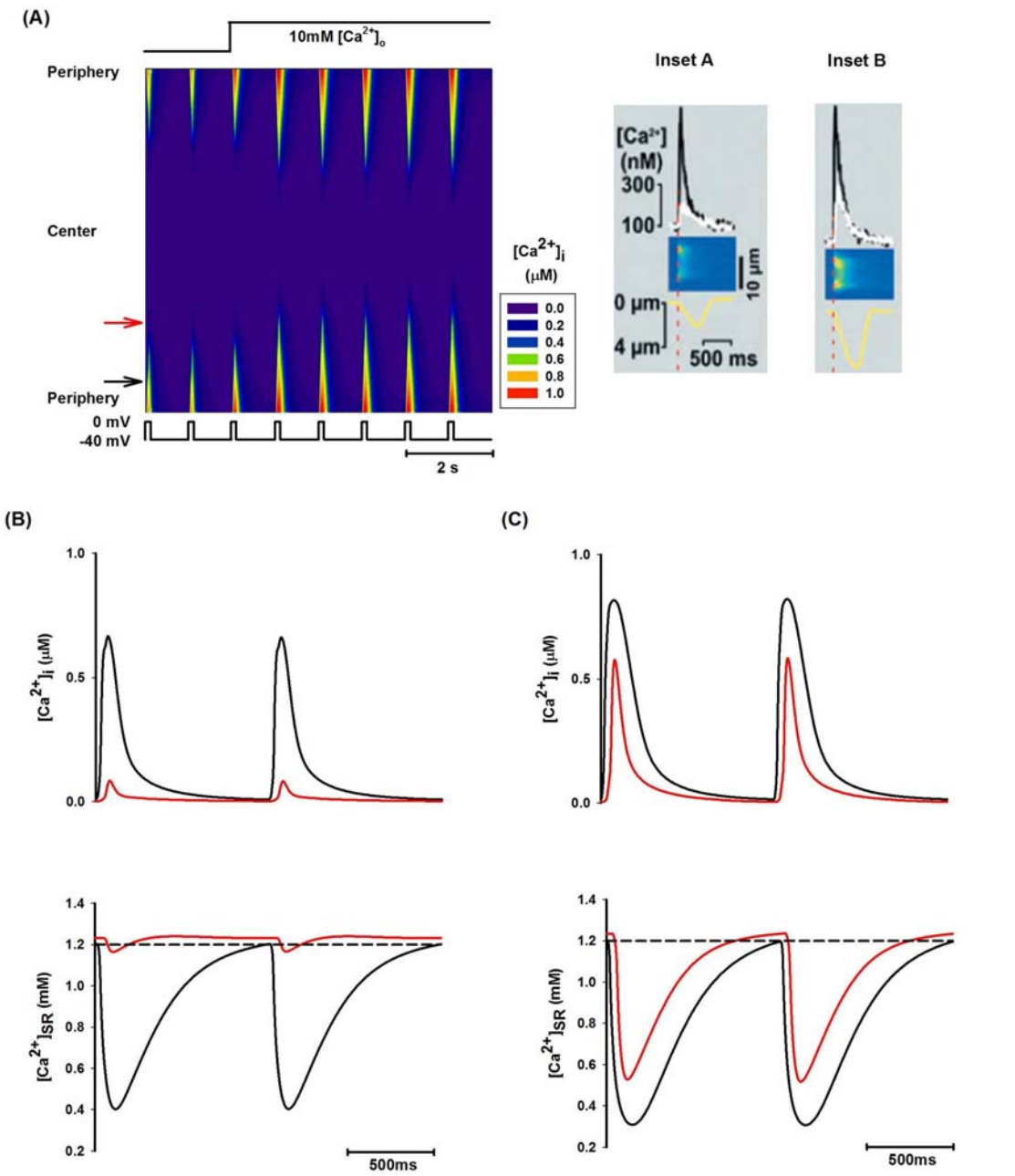

Figure S1. Enhanced Ca^{2+} wave propagation induced by increasing $[Ca^{2+}]_o$. (*A*): The line scan image of cytoplasmic $[Ca^{2+}]_i$ transients. $[Ca^{2+}]_o$ was increased to 10 mM after the first 2 pulses. Inset *A* and *B*: The experimental data of $[Ca^{2+}]_i$ transients before (Inset *A*) and after (Inset *B*) raising $[Ca^{2+}]_o$ from 1 to 10 mM. The inset panels demonstrate the time traces of $[Ca^{2+}]_i$ transients at peripheral (black) and central (white) regions. The line scan images under the traces illustrate spatial $[Ca^{2+}]_i$ transient distribution across the cell. The yellow traces beneath the line scan images show the twitch of the cell. Experimental data was adapted from Mackenzie *et al*. (1). (*B*) and (*C*): Simulation results of $[Ca^{2+}]_i$ (top) and $[Ca^{2+}]_{SR}$ (bottom) recorded from peripheral (back) and central (red) regions of the cell before (*B*) and after (*C*) increasing $[Ca^{2+}]_o$.

2. Effect of increasing RyR sensitivity

Previous experimental studies have shown that increasing the sensitivity of RyR to intracellular Ca^{2+} for CICR (as can be done with a low concentration of caffeine) helps to sustain full Ca^{2+} wave propagation to the central region of atrial myocytes (1). The model was able to reproduce this experimental observation. In simulations, the threshold of RyR for CICR (K_{rel}) was decreased by 10%. In order to exclude possible interactions from varied SR load, the rate of SERCA Ca^{2+} uptake (P_{up}) was increased by 40% to maintain the SR Ca^{2+} content comparable to that in control condition. As enhanced RyR sensitivity enabled efficient CICR in the central region, complete Ca^{2+} wave spread towards the interior region of the cell was observed. Similar to the results of Fig. S1 where Ca^{2+} influx was increased, large $[Ca^{2+}]_i$ transients were sustained throughout the cell upon decreasing K_{rel} (Fig. S2A). Consequentially the amplitude of the $[Ca^{2+}]_i$ transients became homogeneous across the cell as shown in Fig. S2B and S2C. These simulation results (Fig. S2B and S2C) were similar to experimental observations (Inset B) from atrial myocytes devoid of t-tubules (1). The time delays in the $[Ca^{2+}]_i$ and $[Ca^{2+}]_{SR}$ transients between the peripheral and central regions of the cell (Inset A, C and D) demonstrated that the Ca^{2+} wave was first initiated in peripheral regions and then conducted towards the centre of the cell.

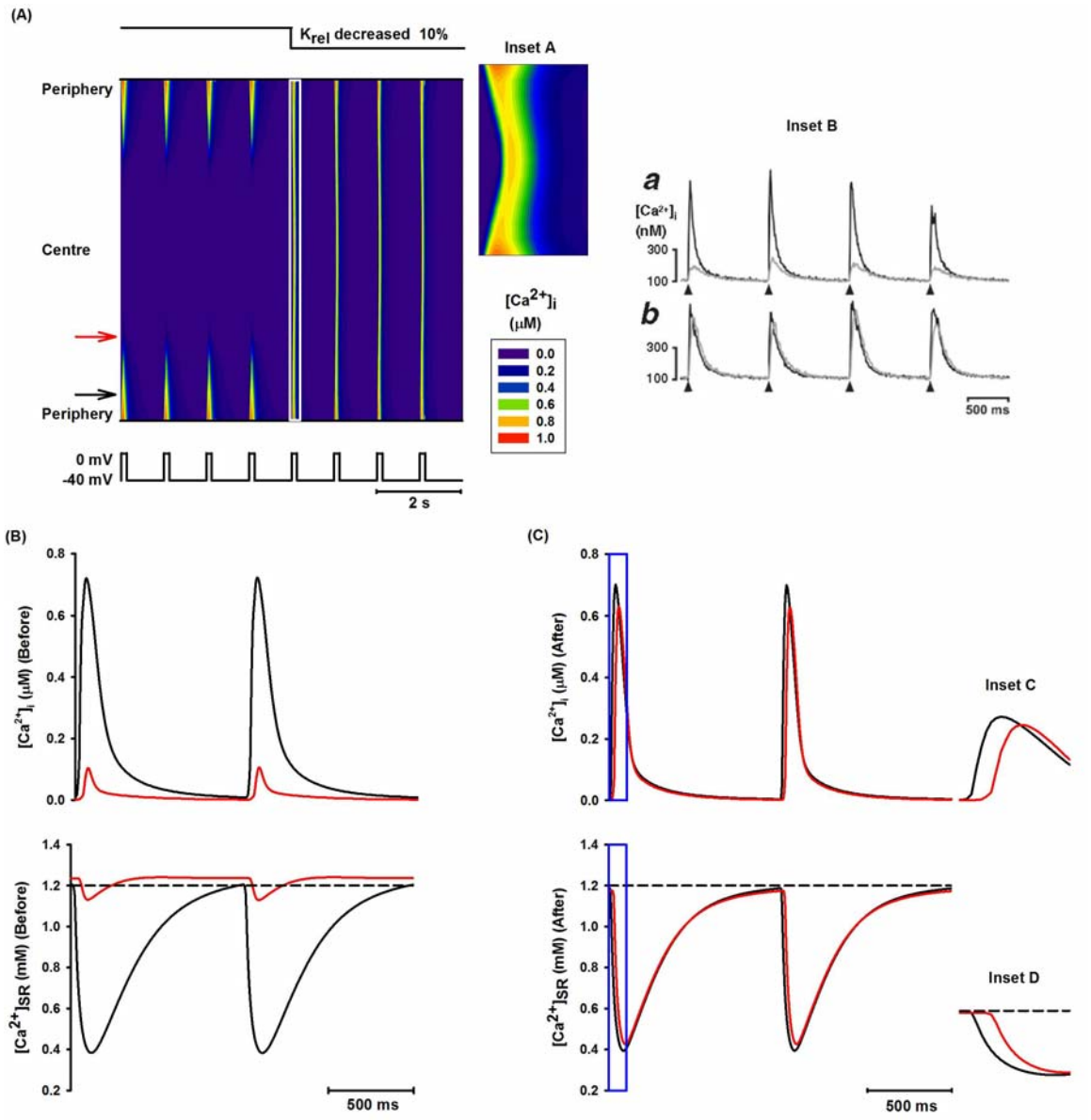

Figure S2. Enhanced Ca^{2+} diffusion induced by decreasing the threshold of RyR for CICR (K_{rel}) to simulate effect of low dose caffeine. (*A*) Line scan image of cytoplasmic Ca^{2+}. The top part of the figure shows K_{rel} protocol. Inset *A*: expanded plot of line scan image for the time period marked by the white box. Inset *B*: The experimental data of peripheral (black) and central (white) $[Ca^{2+}]_i$ transients before (Inset *Ba*) and after (Inset *Bb*) applying 0.1 mM caffeine (1). (*B*) and (*C*): Simulation results of $[Ca^{2+}]_i$ (top) and Ca^{2+} concentration in SR space (bottom) recorded from the peripheral (back) and central (red) regions of the cell before (*B*) and after (*C*) increasing the sensitivity of RyR. Inset *C* and *D*: expanded plots of $[Ca^{2+}]_i$ and $[Ca^{2+}]_{SR}$ for the time period marked by the blue boxes in (*C*), illustrating a phase lag of $[Ca^{2+}]_i$ transients and $[Ca^{2+}]_{SR}$ transients between the peripheral and central elements.

3. Effect of increased SR content

Another experimental technique which can result in full Ca^{2+} wave propagation in atrial myocytes lacking t-tubules is to increase the SR content (1). In order to mimic that effect, the model was first paced for 3 s till a steady state was reached under the control condition. Then the stimulus was stopped for 10 s, during which and afterwards, P_{up} was increased by 75% to enhance the SR Ca^{2+} accumulation. Then the stimulation pulses were reactivated to examine the SR Ca^{2+} concentration and spatial dispersion of $[Ca^{2+}]_i$ transients throughout the cell. As a result, Ca^{2+} waves fully propagated from the periphery into the centre of the cell (Fig. S3A and Inset A) with a spatially homogenous distribution of $[Ca^{2+}]_i$ transients. As shown in Fig. S3B and S3C (bottom panels), such a manoeuvre increases the maximal SR Ca^{2+} concentration by 28.6% in the peripheral region and by 24.1% in the central region as compared to the control condition. This elevated SR Ca^{2+} content promoted Ca^{2+} release in both the peripheral and central regions of the cell (Fig. S3B and S3C; top panels). These simulation results also matched to experimental data (Inset B) obtained from atrial myocytes absent of t-tubules (1). The time delays in the $[Ca^{2+}]_i$ and $[Ca^{2+}]_{SR}$ transients between the peripheral and central regions (Inset A, C and D) indicated that Ca^{2+} signals were initiated in peripheral elements rather than homogeneously throughout the cell.

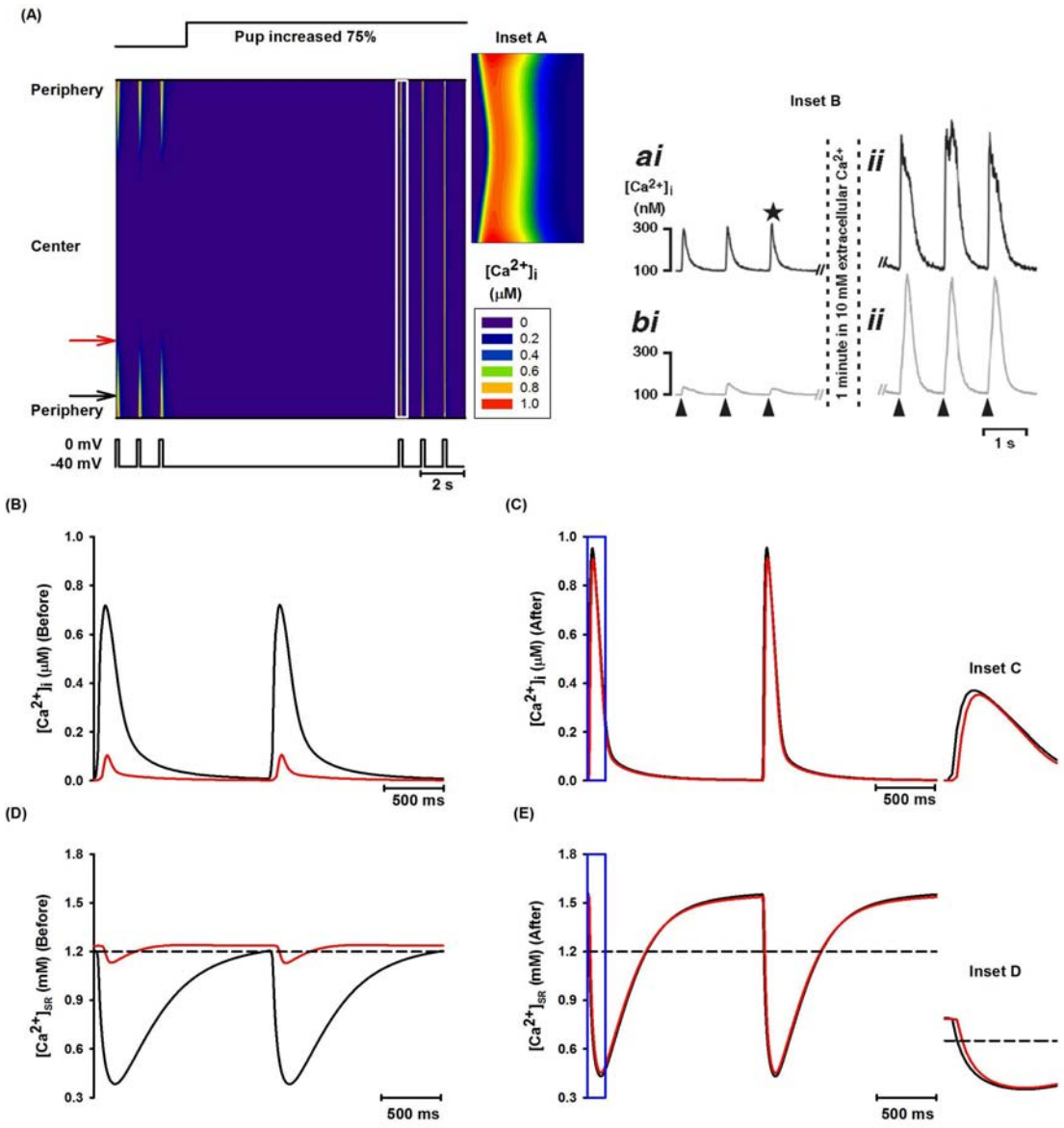

Figure S3. Ca^{2+} wave propagation induced by elevating the SR Ca^{2+} content in atrial myocytes. (*A*): Line scan image of cytoplasmic Ca^{2+}. The SR Ca^{2+} load was elevated by increasing the Ca^{2+} uptake of SR while no stimuli were applied for 10 seconds. Inset *A*: expanded plot of line scan image for the time period marked by the white box, which illustrated that the Ca^{2+} wave was initiated from the peripheral region and then propagated into the central region. Inset *B*: The experimental data of peripheral (Inset *Ba*) and central (Inset *Bb*) $[Ca^{2+}]_i$ transients before (Inset *Bai* and *Bbi*) and after (Inset *Baii* and *Bbii*) increasing the SR content (1). (*B*) and (*C*): Simulation results of $[Ca^{2+}]_i$ (top) and $[Ca^{2+}]_{SR}$ (bottom) recorded from the peripheral (back) and central (red) regions of the cell before (*B*) and after (*C*) increasing the SR content. In panels *B* and *C*, red traces correspond to the position marked by the red arrow in panel *A* while black traces

correspond to the black arrow. Insets *C* and *D*: expanded plots of $[Ca^{2+}]_i$ and $[Ca^{2+}]_{SR}$ for the time periods marked by the blue boxes in panel *C*.

Effect of intra-SR Ca^{2+} diffusion

Previous studies have shown that the SR Ca^{2+} release associated with the SR Ca^{2+} content plays a crucial role in Ca^{2+} wave generation (2, 3). As the refilling of the SR after Ca^{2+} release is associated with the intra-SR Ca^{2+} diffusion (2, 3), in the present study, we examined the effects of the intra-SR Ca^{2+} diffusion on Ca^{2+} wave propagation by modulating the Ca^{2+} diffusion from NSR to JSR. In simulations, the time constant for Ca^{2+} diffusion from NSR to JSR (τ_{tr}) was increased by two times to slow down the Ca^{2+} diffusion between NSR and JSR. As a result, a fully propagating Ca^{2+} wave was followed by a non-propagated wave, which repeated for every two stimulus cycles (Fig. S4A). This was attributable to the slowing down of the Ca^{2+} transportation from NSR and JSR that produced incomplete recovery of the JSR before the next stimulus and thus produced a small Ca^{2+} release (Fig. S4B and S4C). As the Ca^{2+} release was small, no Ca^{2+} wave was induced and therefore, the SR could recover to the level that was able to generate a full Ca^{2+} wave propagation (Fig. S4A and S4C) (4, 5) in the next pacing cycle. All of this process repeated producing Ca^{2+} alternans.

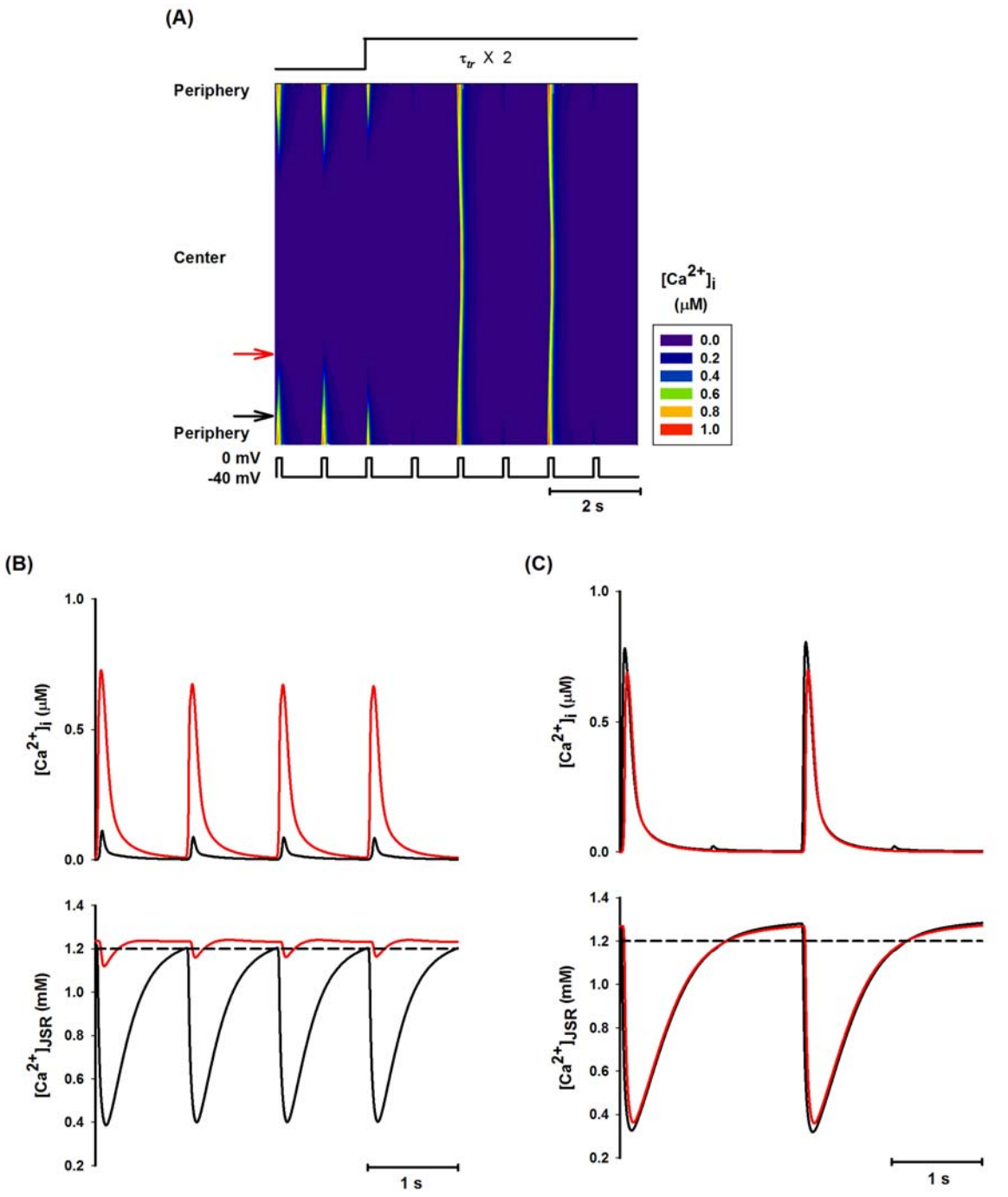

Figure S4. Effect of slowing down Ca^{2+} diffusion from NSR to JSR by increasing the time constant of Ca^{2+} diffusion (τ_{tr}) by two times. (*A*): Line scan image of spatial patterns of $[Ca^{2+}]_i$ transients. (*B*) and (*C*): Traces of $[Ca^{2+}]_i$ transients (top) and Ca^{2+} concentration in SR space (bottom) recorded from peripheral (back) and central (red) regions of the cell before (*B*) and after (*C*) decreasing Ca^{2+} diffusion between NSR and JSR.

Similar alternans was also observed when the Ca^{2+} diffusion between neighbouring NSRs was slowed down (Fig. S5A). This was done by increasing the time constant for Ca^{2+} diffusion between neighbouring NSRs ($\tau_{Ca\_up\_diff}$) by five times. When the inter-element diffusion was slowed down, $[Ca^{2+}]_i$ alternans were produced as shown in Fig. S5C.

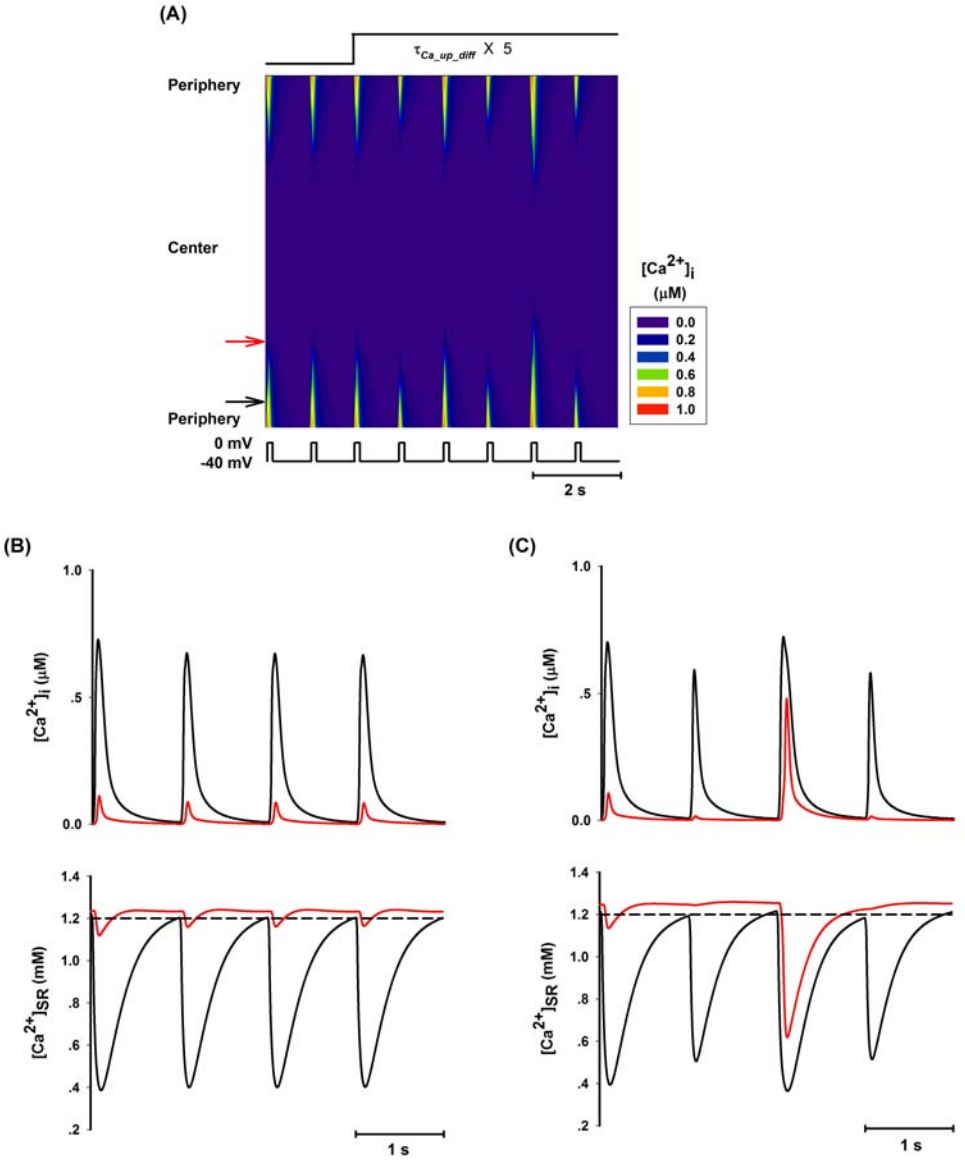

Figure S5. Effect of slowing down Ca^{2+} diffusion between neighbouring NSR by increasing the time constant of Ca^{2+} diffusion ($\tau_{Ca\_up\_diff}$) by five times. (*A*) Line scan of spatial patterns of $[Ca^{2+}]_i$ transients. (*B*) and (*C*) Traces of $[Ca^{2+}]_i$ transients (top) and Ca^{2+} concentration in SR space (bottom) recorded from peripheral (back) and central (red) regions of the cell before (*B*) and after (*C*) decreasing Ca^{2+} diffusion velocity between neighbouring NSR.

Exploring Ca^{2+} alternans in 2D parameter spaces

P_{up}-K_{rel} parameter space. Combined effects of an increased SERCA pump activity and an increased RyR sensitivity on generating $[Ca^{2+}]_i$ alternans were investigated in the P_{up}-K_{rel} parameter space. Results are shown in Fig. S6, which illustrates the regional distribution of $[Ca^{2+}]_i$ alternans in the P_{up}-K_{rel} parameter-space. In Fig. S6A, color from dark blue to bright red represented 1 to 10 different peaks in the measured systolic $[Ca^{2+}]_i$ transient that repeated cyclically, with 1 representing no alternans (Fig. S6B and C), 2 representing 1:1 alternans (Fig. S6D), and large number (n) representing complicated pattern (1:n-1) of alternans (Fig. S6E; 3 different peaks of systolic $[Ca^{2+}]_i$). With a combined modulation of P_{up} and K_{rel}, various patterns of $[Ca^{2+}]_i$ transients were generated in different parameter regions. With a combined increase in both the SERCA pump activity and the sensitivity of RyR to CICR, more spatially homogeneous $[Ca^{2+}]_i$ transients throughout the cell were observed, though the amplitude of systolic $[Ca^{2+}]_i$ decreased (Fig. S6E, 70% of control K_{rel} and 112% of control P_{up}). No $[Ca^{2+}]_i$ alternans were observed when P_{up} was increased by over 50%.

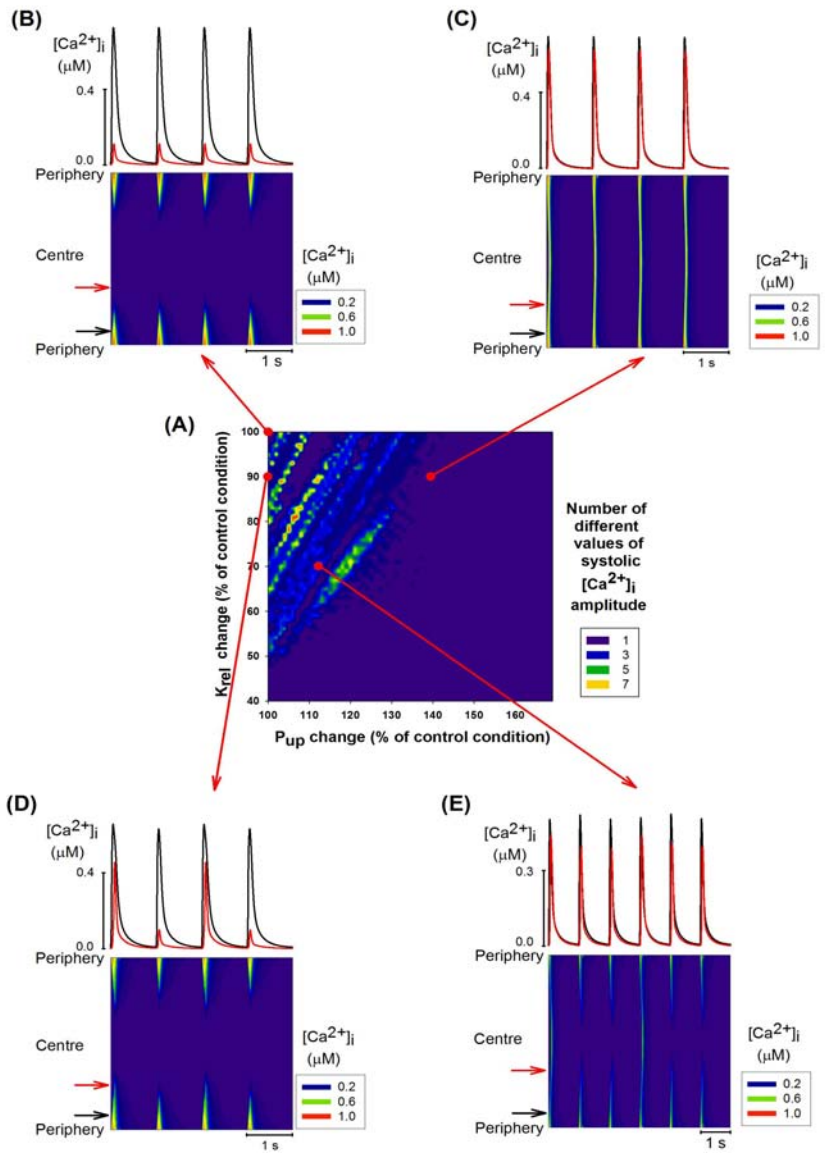

Figure S6. Distribution of systolic Ca^{2+} alternans in the P_{up}-K_{rel} space. (A): Alternans distribution with both increasing P_{up} and decreasing K_{rel}. The degrees of disordered Ca^{2+} transients were color coded in the 2D parameter space. Dark blue stands for steady Ca^{2+} transients from beat to beat as shown in panel *B* and *C*. Red regions stand for unstable or even chaotic Ca^{2+} transients from beat to beat. Panels (*B*) to (*D*) show the detail profiles of Ca^{2+} transients at the sites labelled in 2D parameter space (panel *A*). The top portions of these four panels are the time traces of Ca^{2+} transients in the peripheral and central regions of the cell. The bottom portions are line scan images of cytoplasmic Ca^{2+} transients across the cell. Various patterns of Ca^{2+} transients were illustrated from control condition (panel *B*) to alternating conditions (panel *D* and *E*).

P_{up}-K_{up} space. Combined effects of co-modulating the pump threshold and pump rate of SERCA on generating $[Ca^{2+}]_i$ alternans were investigated in the P_{up}-K_{up} parameter-space. Results were shown in Fig. S7. Fig. S7A illustrates the regional distribution of $[Ca^{2+}]_i$ alternans in the P_{up}-K_{up} space. Various patterns of alternans (1:1:1, Fig. S7B; 1:1, Fig. S7C) were also observed. In addition, a spatial homogenous $[Ca^{2+}]_i$ transient was observed as shown in Fig. S7E.

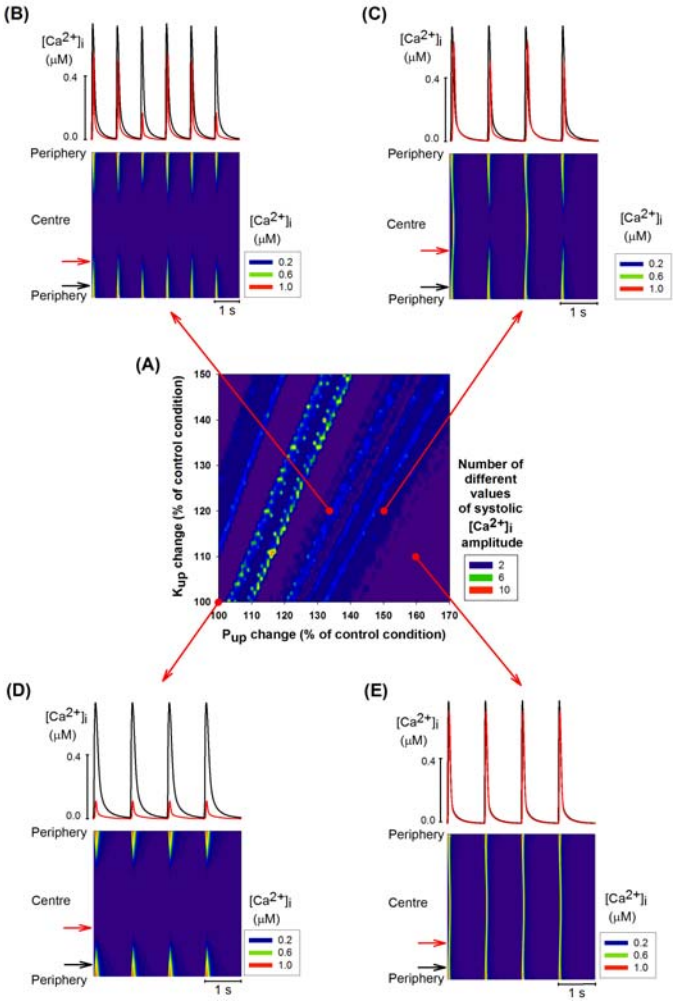

Figure S7. Distribution of systolic Ca^{2+} alternans in P_{up}-K_{up} space. (A) Alternans distribution with increasing both P_{up} and K_{up}. Dark blue regions stand for steady Ca^{2+} transients from beat to beat as shown in panels *D* and *E*. Red regions stand for unstable or even chaotic Ca^{2+} transients from beat to beat. Panels (*B*) to (*D*) show the detail profiles of Ca^{2+} transients at the sites labelled in 2D parameter space (panel *A*). The top portions of these four panels are the time traces of Ca^{2+} transients in the peripheral and central region of the cell. The bottom portions are line scan of cytoplasmic Ca^{2+} transients across the cell.

P_{up}-g_{CaL} space. Combined effects of increased Ca^{2+} influx with an increased SERCA pump activity on generating $[Ca^{2+}]_i$ alternans were investigated in the P_{up}-g_{CaL} parameter space. Results were shown in Fig. S8. Complex patterns of systolic $[Ca^{2+}]_i$ profiles were mainly present in two areas: left bottom and top right corners as shown in panel A. Fig. S8D represents the control condition and Fig. S8C showed an enhanced Ca^{2+} propagation wave and a spatial homogenous $[Ca^{2+}]_i$ distribution in the cell with a modest increase in the Ca^{2+} influx, but a significant increase in the SERCA pump activity. When both the Ca^{2+} influx and SERCA pump activity were modestly increased, 1:1 $[Ca^{2+}]_i$ alternans were observed with more dramatic effects seen in the central region (Fig. S8E).

It was shown that the disordered $[Ca^{2+}]_i$ transient observed in the left bottom (close to the control condition) and the top right corner regions (significantly increased P_{up} and g_{CaL}) of P_{up}-g_{CaL} parameter space were completely different. With dramatic increases in both the Ca^{2+} influx and the SR uptake efficiency, a spontaneous second Ca^{2+} release occurred in response to one stimulus as shown in Fig. S8B due to the SR Ca^{2+} overload.

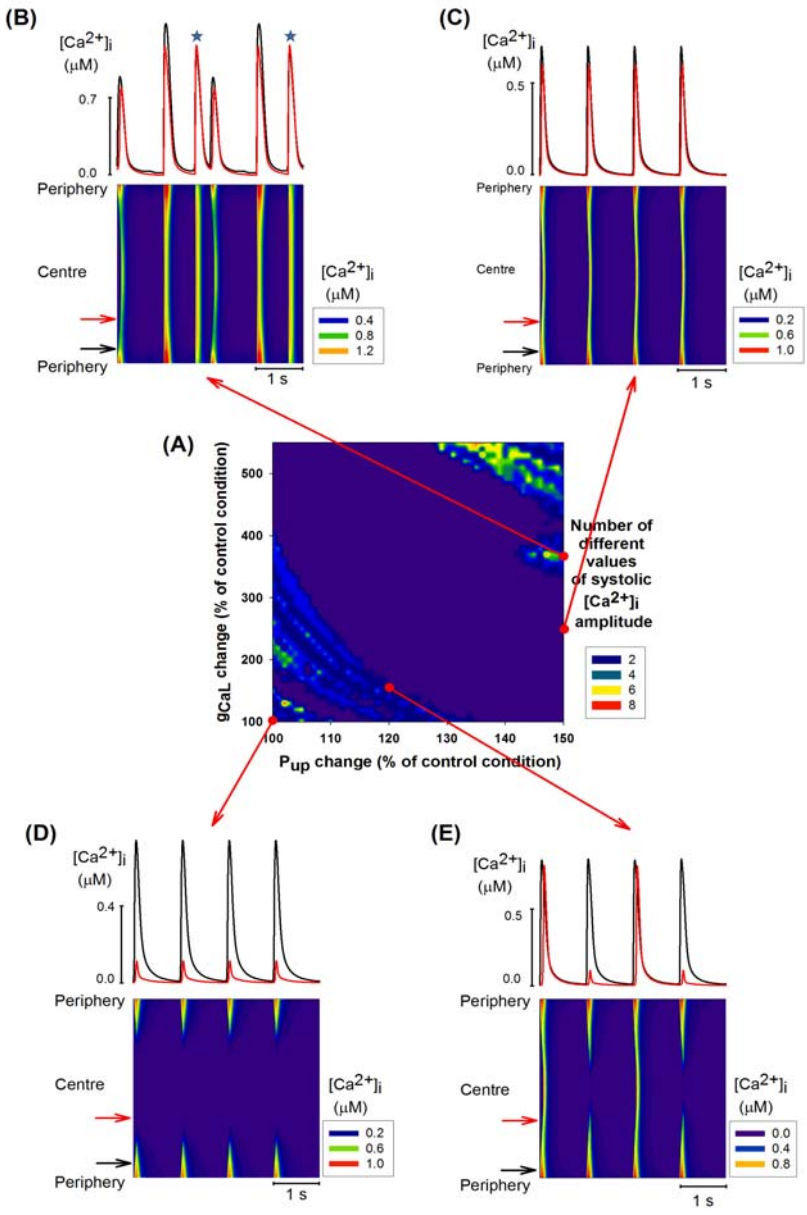

Figure S8. Distribution of systolic Ca^{2+} alternans in P_{up}-g_{CaL} space. (*A*) Alternans distribution with increasing both P_{up} and g_{CaL}. Dark blue regions stand for steady Ca^{2+} transients from beat to beat as shown in panels *C* and *D*. Red regions stand for unstable even chaotic Ca^{2+} transients from beat to beat. Panels (*B*) to (*E*) show the detail profiles of Ca^{2+} transients at the sites labelled in 2D parameter space (panel *A*). The top portions of these four panels are the time traces of Ca^{2+} transients in the peripheral and central region of the cell. The bottom portions are line scan of cytoplasmic Ca^{2+} transients across the cell. In panel *B*, a second Ca^{2+} release during the same stimulation interval is marked by the asterisk.

Roles of Ca^{2+} handling kinetics – insights from 2-parameter analysis. Analyses based on 2-parameter spaces provided other meaningful insights into the generation of Ca^{2+} alternans when two parameters associated with Ca^{2+} cycling kinetics were co-modulated. For example, results shown in Fig. S6 and S8 in P_{up}-K_{rel} and P_{up}-g_{CaL} parameter spaces indicated that increasing P_{up} (the rate for Ca^{2+} uptake by SR Ca^{2+} pumps) tended to suppress the genesis of Ca^{2+} alternans that would be generated if g_{CaL} or K_{rel} was modulated alone. This may be explained by the fact that an increased SR uptake allowed the SR content to be refilled with relative ease to such a level that produced a large Ca^{2+} release, avoiding the genesis of alternans (Fig. S6 and S8). Interestingly, when P_{up} was increased over a certain value in both of the P_{up}-g_{CaL} and P_{up}-K_{rel} parameter spaces, no alternans were observed. However, in the P_{up}-K_{up} space, alternans were observed in most of the parameter region (Fig. S7), indicating that a defected SR uptake due to an elevated threshold played a more significant role in generating Ca^{2+} alternans, which could not be counter-balanced by increased maximal pump activity of the SERCA (P_{up}).

References

1. Mackenzie, L., H. L. Roderick, M. J. Berridge, S. J. Conway, and M. D. Bootman. 2004. The spatial pattern of atrial cardiomyocyte calcium signalling modulates contraction. *J. Cell. Sci*. 117:6327-37.
2. Zima, A. V., E. Picht, D. M. Bers, and L. A. Blatter. 2008. Termination of cardiac Ca^{2+} sparks: role of intra-SR $[Ca^{2+}]$, release flux, and intra-SR Ca^{2+} diffusion. *Circ. Res.* 103(8):e105-15.
3. Lukyanenko, V., S. Subramanian, I. Gy□rke, T. F.Wiesner, and S. Gy□rke. 1999. The role of luminal Ca^{2+} in the generation of Ca^{2+} waves in rat ventricular myocytes. *J. Physiol.* 518(1):173-86.
4. Diaz, M. E., S. C. O'Neill, and D. A. Eisner. 2004. Sarcoplasmic reticulum calcium content fluctuation is the key to cardiac alternans. *Circ. Res.* 94:650-656.
5. Tao, T., S. C. O'Neill, M. E. Diaz, Y. T. Li, D. A. Eisner, and H. Zhang. 2008. Alternans of cardiac calcium cycling in a cluster of ryanodine receptors: A simulation study. *Am. J. Physiol.* 295:H595-H609.